JOURNAL OF ENVIRONMENTAL SCIENCES 76 (2019) 133–141

Available online at www.sciencedirect.com

ScienceDirect

www.elsevier.com/locate/jes

JES JOURNAL OF ENVIRONMENTAL SCIENCES

www.jesc.ac.cn

Evaluation of natural goethite on the removal of arsenate and selenite from water

*Andrew T. Jacobson, Maohong Fan**

Department of Chemical Engineering, University of Wyoming, Laramie, WY 82071, USA

ARTICLE INFO

Article history:
Received 19 February 2018
Revised 17 April 2018
Accepted 18 April 2018
Available online 30 April 2018

Keywords:
Arsenic
Selenium
Adsorption
Desorption
FeOOH
Water treatment

ABSTRACT

Elevated arsenic and selenium concentrations in water cause health problems to both humans and wildlife. Natural and anthropogenic activities have caused contamination of these elements in waters worldwide, making the development of efficient cost-effective methods in their removal essential. In this work, removal of arsenate and selenite from water by adsorption onto a natural goethite (α-FeOOH) sample was studied at varying conditions. The data was then compared with other arsenate, selenite/goethite adsorption systems as much of literature shows discrepancies due to varying adsorption conditions. Characterization of the goethite was completed using inductively coupled plasma mass spectrometry, X-ray diffraction, Fourier-transform infrared spectroscopy, scanning electron microscopy, and Brunauer–Emmett–Teller surface area analysis. Pseudo-first order (PFO) and pseudo-second order (PSO) kinetic models were applied; including comparisons of different regression methods. Various adsorption isotherm models were applied to determine the best fitting model and to compare adsorption capacitates with other works. Desorption/leaching of arsenate and selenite was studied though the addition of phosphate and hydroxyl ions. Langmuir isotherm modeling resulted in maximum adsorption capacities of 6.204 and 7.740 mg/g for arsenate and selenite adsorption, respectively. The PSO model applied with a non-linear regression resulted in the best kinetic fits for both adsorption and desorption of arsenate and selenite. Adsorption decreased with increasing pH. Phosphate induced desorption resulted in the highest percentage of arsenate and selenite desorbed, while hydroxide induced resulted in the fastest desorption kinetics.
© 2018 The Research Center for Eco-Environmental Sciences, Chinese Academy of Sciences.
Published by Elsevier B.V.

Introduction

Arsenic and selenium present in contaminated waters exist predominately as inorganic arsenite, arsenate, selenite, and selenate corresponding to the oxidation states of +3, +5, +4, and +6, respectively. Arsenate and arsenite are very toxic to humans and wildlife when ingested, causing cancer to the bladder, lungs, kidney, liver, and skin as well as causing other ailments (Choong et al., 2007). Ingestion of selenium in large quantities can cause selenosis, resulting in death for severe cases (Frankenberger Jr. and Benson, 1994). Due to the toxicity and prevalence of arsenic, the EPA (Environmental Protection Agency) and WHO (World Health Organization) regulations state a maximum contaminant level (MCL) of 10 μg/L (WHO, 2011; EPA, 2017a) for drinking water. Similarly, the EPA has an MCL set to 50 μg/L (EPA, 2017b) for selenium in drinking water. Furthermore, in 2016 the EPA extended selenium guidelines to all freshwater under The Aquatic Life Ambient Quality Criteria for selenium in freshwater, providing recommendations to states for selenium criteria under the Clean Water Act (EPA, 2016).

* *Corresponding author. E-mail:* mfan@uwyo.edu (Maohong Fan).

https://doi.org/10.1016/j.jes.2018.04.016
1001-0742/© 2018 The Research Center for Eco-Environmental Sciences, Chinese Academy of Sciences. Published by Elsevier B.V.

Numerous methods for the removal of arsenic and selenium from aquatic environments have been studied including coagulation, flocculation, ion exchange, precipitation, membrane filtration, ozone oxidation, biological treatment, electrochemical treatment, and adsorption (Choong et al., 2007; Golder Associates Inc., 2009). Of these, adsorption is very encouraging on account of its simplicity and effectiveness for point-of-use applications. Many materials for adsorption of both selenium and arsenic have been studied, with metal oxides being most common due to their universality (Mohan and Pittman, 2007; Golder Associates Inc., 2009). Particularly, iron based adsorbents have received much attention (Giles et al., 2011; Duc et al., 2003), and of these goethite (α-FeOOH) has shown high potential. The large particle size, natural ubiquity, coagulant potential, and low cost of goethite have given it attention in many water remediation applications. Both synthetic and natural goethite samples have been researched in their selenium and arsenic adsorption potentials (Ladeira and Ciminelli, 2004; Balistrieri and Chao, 1987; Matis et al., 1997; Parida et al., 1997; Giménez et al., 2007; Rovira et al., 2008). The adsorption capacitates vary between each synthetic as well as each natural goethite sample due to changing material properties and experimental conditions.

In this work, an unstudied natural goethite (α-FeOOH) sample was characterized and evaluated for the removal of arsenate and selenite from water. The results were then compared with other As(V) + Se(IV)/goethite adsorption systems.

1. Methods and materials

1.1. Chemicals

Natural goethite (α-FeOOH) was purchased through Alpha Chemicals as natural yellow iron oxide. The arsenate and selenite used in the experiments were purchased from Inorganic Ventures at a concentration of 1000 mg/L As(V) and 1000 mg/L Se(IV). The desired concentrations of selenite and arsenate for the adsorption batch experiments were achieved by dilution with deionized water. Fisher Scientific American Chemical Society (ACS) 36.5%–36.0% HCl, Fisher TraceMetal 67.0%–70.0% HNO_3, SigmaAldrich 48.0% HF, and VWR ACS grade 99.5% boric acid were used for goethite digestions. For desorption experiments Fisher ACS 97.0% NaOH, Fisher ACS 99.0% Na_2HPO_4, Fisher ACS 98.0% $NaH_2PO_4{\cdot}H_2O$, and Sigma 85.0% H_3PO_4 were used.

1.2. Instrumentation

An X-ray diffraction (XRD) system (Smartlab, Rigaku, Japan) using a Cu Kα1 line (1.5406 Å) operating at 40 kV/40 mA, with 2θ ranging from 10° to 90° was used for the X-ray diffraction analysis. The field emission scanning electron microscope (SEM) (Quanta 450, FEI, USA) was equipped with a Schottky field emission gun at an accelerating voltage of 20 kV. The BET (Brunauer–Emmett–Teller) surface area and BJH (Barrett–Joyner–Halenda) pore volume were acquired using an automated gas sorption analyser (Autosorb IQ, Quantachrome, USA). Infrared analysis was done using an attenuated total reflectance Fourier-transform infrared (ATR-FTIR) spectrometer (Nicolet iS50, Thermo Scientific, USA). For elemental analysis an inductively coupled plasma mass spectrometer (ICP-MS) was used in standard mode (NexION 300S, PerkinElmer, USA).

1.3. Experiments

The adsorption experiments for both arsenate and selenite were completed in 6 L polyvinyl chloride batch reactors equipped with mechanical stirrers. A large lab scale volume of 6 L was chosen to closer simulate real world point-of-use application for a more accurate scale up of the results. Stirring speeds were varied with no significant change in adsorption occurring. Kinetic studies were completed at initial adsorbate concentrations (C_0) varying between 50 and 250 μg/L, and all other experiments were set at 150 μg/L. Isotherm studies were completed at goethite suspensions of 0.010–0.500 g/L, and all other experiments were done at a suspension of 0.333 g/L. All experiments were completed at a pH of 4, excluding pH effect studies where NaOH and HNO_3 were used to set the pH. Spent goethite was filtered and dried for use in desorption studies. For desorption, to reach a pH of 3 and 7 while maintaining a PO_4^{3-} concentration of 0.1 mol/L, a 9:1 by volume mixture of 0.1 mol/L $NaH_2PO_4{\cdot}H_2O$:0.1 mol/L H_3PO_4 and 1:1 by volume 0.1 mol/L $NaH_2PO_4{\cdot}H_2O$:0.1 mol/L Na_2HPO_4 were used, respectively. For the desorption studies at higher pH values, 1 mol/L NaOH was used to increase the pH. The digestion of goethite for chemical analysis consisted of 0.1 g goethite being added to 16 g of a 1:2:1 by mass mixture of HF (49%), HCl (38%), and HNO_3 (69%), respectively. The mixture was then heated to 80°C in a silicone oil bath. Once all solids had dissolved the mixture was removed from heat and 4 g of boric acid was added to complex the excess fluoride ions. The mixture was then diluted to 100 g with deionized (DI) water.

2. Results and discussion

2.1. Goethite characterization

Elemental analysis of the goethite established the presence of silicone, aluminium, manganese, potassium, magnesium, calcium, and sodium. These results are displayed in Table 1. The XRD pattern of the natural goethite is shown in Fig. 1. The characteristic peaks of goethite can be seen at 2θ values of 17.8°, 21.2°, 33.2°, 36.7°, 53.2°, and 59.0°. The peaks at 35.1°, 43.4°, and 57.5° are distinctive to corundum and those at 26.7° and 50.1° to quartz (Joint Committee on Powder Diffraction Standards, 1980). When compared to the references, the quartz peak at 2θ of 26.7° is much larger due to the higher concentration of quartz in this studies goethite sample. In conjunction with XRD, ICP-MS elemental analysis revealed the concentration of goethite as 55.44% ± 0.44% by mass in the natural sample as no other iron oxide species were present in the XRD pattern, including akaganeite (β-FeOOH), lepidocrocite (γ-FeOOH), hematite (Fe_2O_3), and magnetite (Fe_3O_4) (Joint Committee on Powder Diffraction Standards, 1980). This is also in agreement with the vendor analysis of 55% goethite. FTIR results are shown in Fig. 2, where fresh, arsenate loaded, and selenite loaded goethite was characterized. FTIR analysis contributed to the confirmation of goethite in the natural sample. The broad peak located and 3130 cm^{-1} corresponds to

Table 1 – Inductively coupled plasma mass spectrometer elemental analysis of the natural goethite.

Goethite composition (wt.%)		
Component	Experimental analysis	Vendor analysis
Fe	34.85 ± 0.28	–
Si	17.73 ± 0.19	–
Al	3.25 ± 0.07	–
Mn	2.05 ± 0.03	2.30
K	1.64 ± 0.02	–
Mg	0.50 ± 0.01	–
Ca	0.13 ± 0.01	–
Na	0.07 ± 0.001	–
FeOOH	55.44 ± 0.44	55.00
SiO_2	–	25.00
Al_2O_3	–	6.00
MnO_2	–	3.60

the –OH stretching vibration of goethite, while the peaks at 798 and 905 cm^{-1} can be attributed to the out of plane and in plane bending vibrations of –OH, respectively (Farmer, 1974; Prasad et al., 2006). The peak at 467 cm^{-1} is either due to Si–O asymmetrical bending or an FeO_6 lattice (Prasad et al., 2006; Müller et al., 2014). The peak at 1020 cm^{-1} can be described by the asymmetric stretching vibration of Si–O in quartz and/or other silicone compounds (Farmer, 1974; Müller et al., 2014). Comparison of the fresh and spent goethite samples shows no major differences, signifying the stability of the natural goethite sample after adsorption. Peaks related to arsenate and selenite adsorption are not observed due to their low concentrations. The acicular crystal agglomerates common of goethite (Duc et al., 2003) can be seen in the SEM images of Fig. 3. The images

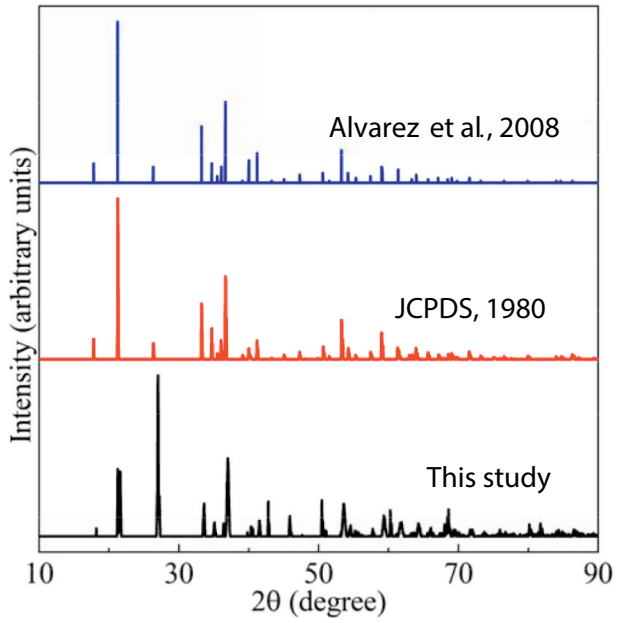

Fig. 1 – X-ray diffraction patterns of the natural goethite in this study, Joint Committee on Powder Diffraction Standards (JCPDS), 1980, and Alvarez et al., 2008.

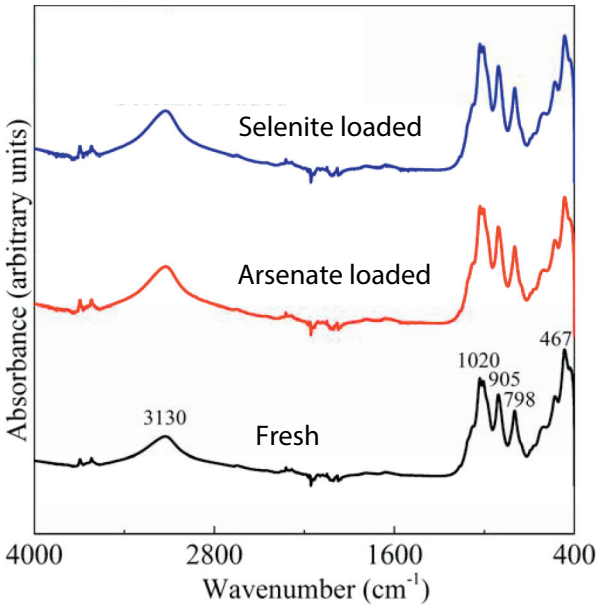

Fig. 2 – Fourier-transform infrared spectroscopy images of fresh, arsenate loaded, and selenite loaded natural goethite.

also show that no changes to the morphology of the goethite have occurred after adsorption. BET surface area analysis of the goethite revealed a surface area of 13.133 m^2/g and a BJH pore volume of 0.068 cm^3/g. Through sieve analysis the average particle size was found to be 37 μm.

2.2. Adsorption kinetics

In this work, pseudo-first order (PFO) and pseudo-second order (PSO) rate laws were applied and compared at varying initial adsorbate concentrations to study the adsorption kinetics of arsenate and selenite on the natural goethite sample. The integrated PFO rate expression of Lagergren (Lagergren, 1898) is of the form:

$$q_t = q_a\left(1-e^{-k_1 t}\right) \quad (1)$$

where k_1 (hr^{-1}) is the rate constant of adsorption, q_a (mg/g) is the amount of solute adsorbed at equilibrium, and q_t (mg/g) is the amount of solute adsorbed at time t (hr). The integrated PSO rate expression (Ho and McKay, 1999) used is as follows:

$$q_t = \frac{q_a^2 k_2 t}{1 + q_a k_2 t} \quad (2)$$

where k_2 (g/(mg·hr)) is the rate constant of adsorption. For many adsorption systems the PFO and PSO models have been applied through linear regressions by plotting $\ln(q_a - q_t)$ *vs.* t and t/q_t *vs.* t, respectively and solving for the kinetic parameters from the slopes and intercepts of the regressions. It has been shown that the linear regression is bias towards the PSO model (Simonin, 2016). Therefore, regressions were completed using not only a two-parameter linear regression, but also one-parameter and two-parameter non-linear regressions with an optimized Levenberg–Marquardt method in Mathcad 15®. This linear

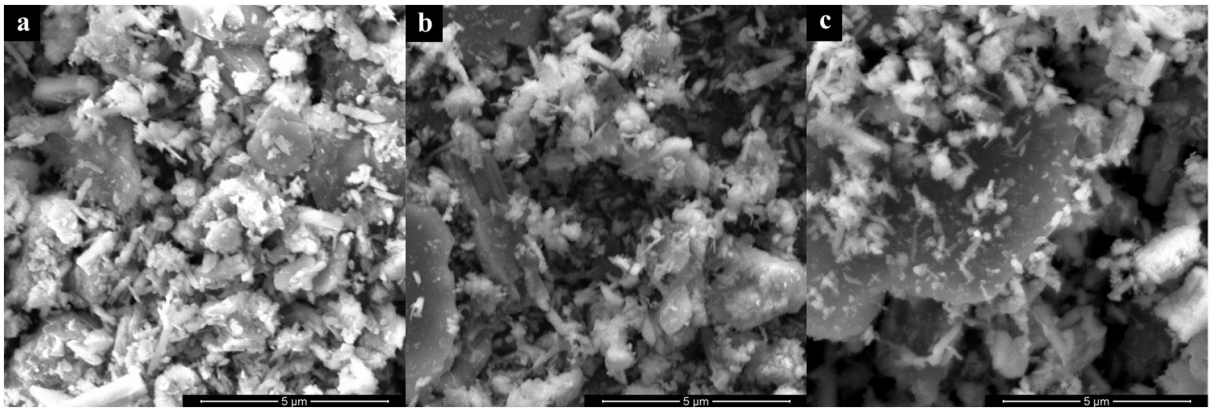

Fig. 3 – Scanning electron microscope images of (a) fresh, (b) selenite loaded, and (c) arsenate loaded natural goethite.

regression bias was confirmed when comparing the R^2 values of the linear and non-linear regressions. For arsenate and selenite adsorption, the PFO model resulted in poor fits ($R^2 < 0.7000$) using linear regressions, but provided fits of $R^2 > 0.9000$ for the non-linear regressions. The two-parameter non-linear regressions gave the best R^2 values, but since q_a was known from experimental data, the one-parameter non-linear regressions were chosen to compare the PFO and PSO models and calculate k. In both arsenate and selenite adsorption the PSO model had the best fit (Fig. 4) for all but one initial adsorbate concentration. This concentration, 233.2 µg/L arsenate, had a better fit using the PFO model. This suggests that at larger initial concentrations of arsenate a PFO model may be a better fit when using a non-linear regression. Also this may be the case for selenite, as the higher initial adsorbate concentrations resulted in better PFO fits. The kinetic parameters derived from the PSO one-parameter regressions are displayed in Table 2.

2.3. Adsorption isotherms

The adsorption isotherms were characterized using three models, *i.e.*, Langmuir, Freundlich, and Dubinin–Rasushkevich (D–R). The Langmuir (Langmuir, 1916; Foo and Hameed, 2010) model can be expressed as:

$$q_e = \frac{q_m b C_e}{1 + b C_e} \tag{3}$$

where C_e (mg/L) is the adsorbate equilibrium concentration in solution, q_e (mg/g) is the equilibrium adsorbed concentration, q_m (mg/g) is the maximum monolayer coverage capacity, and b

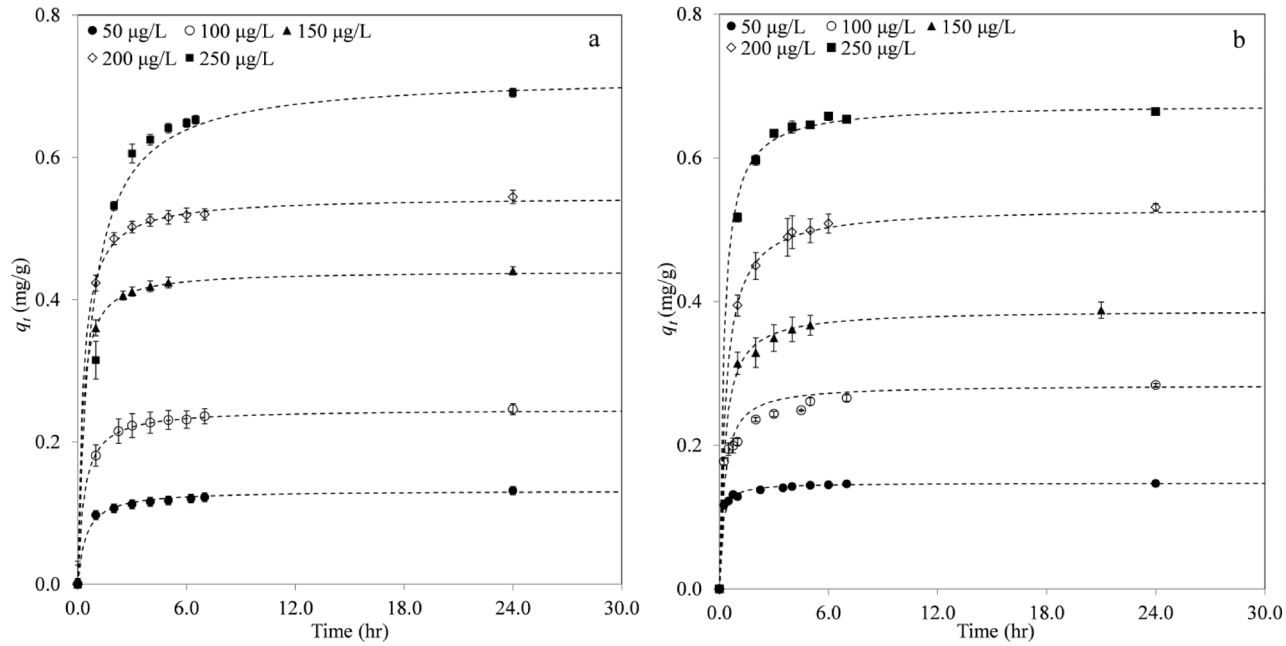

Fig. 4 – Pseudo-second order (PSO) kinetic fits of adsorption at varying initial concentrations of (a) arsenate and (b) selenite onto a 0.333 g/L goethite suspension at a pH 4. q_t: solute adsorbed at time t.

Table 2 – Kinetics parameters of arsenate and selenite adsorption at varying initial adsorbate concentrations (C_0) regressed from the one-parameter non-linear pseudo-second order (PSO) rate law.

C_0 (μg/L)	k (g/(mg·hr))	q_a (mg/g)	R_1^2	R_2^2
Arsenate adsorption				
50.7	17.401	0.131	0.9241	0.9942
90.3	11.914	0.246	0.9720	0.9994
149.1	10.449	0.440	0.9855	0.9998
197.6	6.755	0.544	0.9789	0.9994
233.2	1.711	0.691	0.9912	0.9622
Selenite adsorption				
52.1	20.852	0.147	0.9521	0.9930
102.0	13.926	0.284	0.7728	0.9478
135.4	9.286	0.388	0.9647	0.9972
185.5	5.584	0.531	0.9755	0.9992
227.2	6.251	0.674	0.9900	0.9965

k: PSO rate constant; q_a: Solute adsorbed at equilibrium. R_1^2 and R_2^2: the fits for pseudo-first and pseudo-second order rate laws, respectively.

(L/mg) is the equilibrium adsorption constant linked to the affinity of binding sights of the adsorbent. The dimensionless constant separation factor (R_L) is used to quantify the effectiveness of an adsorbent in removal of an adsorbate. R_L is evaluated through the expression:

$$R_L = \frac{1}{1 + bC_0} \tag{4}$$

where C_0 (mg/L) is the initial adsorbate concentration in solution. The Freundlich isotherm model (Freundlich, 1906; Foo and Hameed, 2010) was also applied as:

$$q_e = K_f C_e^{\frac{1}{n}} \tag{5}$$

with K_f (mg/g) being the Freundlich isotherm constant related to adsorption capacity and n is the adsorption intensity. Unlike Langmuir, the Freundlich isotherm is not restricted to the formation of a monolayer and can be applied to multilayer adsorption. Last, the Dubinin–Rasushkevich (D–R) isotherm model (Dubinin and Radushkevich, 1947; Foo and Hameed, 2010) was applied:

$$q_e = q_s e^{-k_{ad}\varepsilon^2} \tag{6}$$

where q_s (mg/g) is the theoretical isotherm saturation capacity, and k_{ad} (mol^2/kJ^2) and ε are the Dubinin–Rasushkevich isotherm constants with ε equal to:

$$\varepsilon = RT \ \ln\left(1 + \frac{1}{C_e}\right) \tag{7}$$

where R is the gas constant and T (K) the absolute temperature. The D–R model is often used to determine the adsorption mechanism through the mean free energy of adsorption per molecule transferred to the surface from infinity (E (kJ/mol)):

$$E = \sqrt{\frac{1}{2k_{ad}}} \tag{8}$$

All isotherm experiments were run for 72 hr to ensure equilibrium was reached. Fig. 5 shows equilibrium was reached within 24 hr for all goethite suspensions, with the higher suspensions reaching equilibrium in less than 5 hr. Linear and non-linear regressions were applied for the isotherm fits. Linear regressions were performed by plotting q_e^{-1} *vs.* C_e^{-1}, $\ln(q_e)$ *vs.* $\ln(C_e)$, and $\ln(q_e)$ *vs.* ε^2 for Langmuir, Freundlich, and D–R isotherms, respectively. The isotherm parameters were then solved for from the regressed slopes and intercepts. To compare the three models applied it is common to use the R^2 values from linear regressions. This, however, is inappropriate as according to statisticians (Scott and Wild, 1991) the models should be

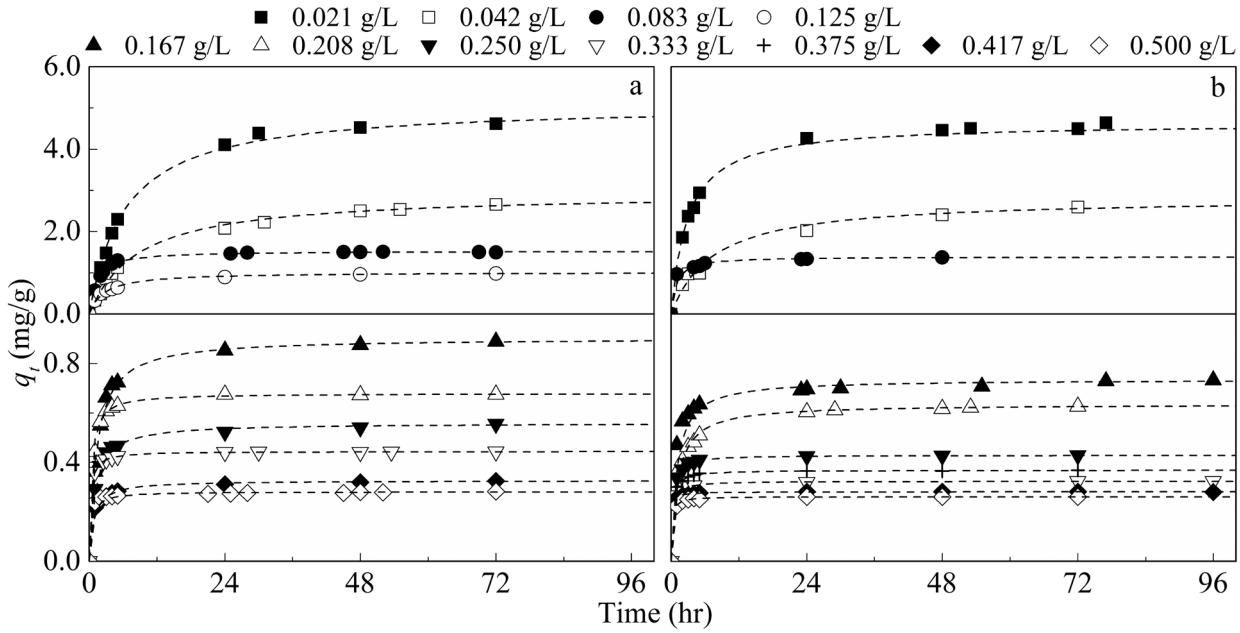

Fig. 5 – PSO kinetic fits of the equilibrium experiments used in isotherm modeling at pH 4 and initial adsorbate concentrations (C_0) 150 μg/L.

Table 3 – Isotherm parameters of arsenate and selenite adsorption derived using non-linear regressions.

Model	Parameters	Arsenate	Selenite
Langmuir	q_m (mg/g)	6.204	7.740
	R_L	0.109	0.334
	R^2	0.9722	0.9860
Freundlich	K_f (mg/g)	18.482	28.053
	n	2.016	1.327
	R^2	0.9709	0.9640
Dubinin-Rasushkevich	q_s (mg/g)	7.905	8.135
	E (kJ/mol)	6.914	5.332
	R^2	0.9783	0.9882

q_m: Langmuir adsorption capacity; R_L: separation factor; K_f: Freundlich isotherm constant; n: adsorption intensity; q_s: Dubinin–Rasushkevich adsorption capacity; E: mean free energy of adsorption.

compared in the same scale, not the transformed ones; therefore, all R^2 values were compared in the scale of Eqs. (5), (7), and (8). The non-linear regressions were computed using an optimized Levenberg–Marquardt method in Mathcad 15®. Linear and non-linear regressions gave comparable results for the isotherm parameters; however for all three models the R^2 values for the non-linear regressions were higher than those of the linear regression in both arsenate and selenite adsorption and therefore were used for reporting the isotherm constants in Table 3. Among these the best fit for arsenate and selenite adsorption was the D–R model at an R^2 of 0.9783 and 0.9882, respectively. This was closely followed by the Langmuir model then by the Freundlich for both systems. Maximum capacities of the D–R and Langmuir models were close for both adsorption systems. The dimensionless Langmuir constant separation factor (R_L) was between zero and one for arsenate and selenite adsorption, signifying favorable non-reversible adsorption. The Langmuir isotherm fit indicates monolayer coverage. For both systems, the mean free energy (E) calculated from the D–R isotherm model was close to the 8–16 kJ/mol value that indicates chemisorption by ion-exchange (Ho et al., 2002). This ion-exchange mechanism is in agreement with previous works (Dzombak and Morel, 1990). Furthermore, this chemisorption/ion-exchange has been found to result in the formation of inner-sphere complexes for arsenate (Ladeira and Ciminelli, 2004) and a mixture of inner and outer-sphere complexes for selenite (Giménez et al., 2007).

Table 4 shows the calculated Langmuir adsorption capacities for both arsenate and selenite on goethite in this work compared with other findings for the As(V) + Se(IV)/goethite adsorption systems. Synthetic and natural goethite samples are compared. The arsenate removal capacity of the natural goethite in this work is about half of one of the natural goethite samples from previous works (Ladeira and Ciminelli, 2004). This is mainly due to the increased concentration of goethite in their natural sample (85% *vs.* 55%). Another natural sample (Giménez et al., 2007) showed a much lower arsenate capacity then this work and others. This may be due to the lower surface area and unknown goethite content of the natural sample. The synthetic goethite sample showed the highest capacity (Matis et al., 1997). This can be explained by the low pH used, high goethite content, and high surface area. As for selenite adsorption similar results were found. The highest adsorption capacity is with a high surface area synthetic goethite (Parida et al., 1997). One other study was found for natural goethite as an adsorbent in Se(IV) removal (Rovira et al., 2008). In their work the same natural goethite used by Giménez et al. (2007) for arsenate adsorption was studied for selenite. The capacity was found to be quite lower than that of the natural sample used in this study. This again may be attributed to the low surface area and unknown goethite content of the natural sample.

2.4. Effect of pH on selenite and arsenate adsorption

Adsorption of arsenate and selenite was investigated at pH values ranging from 3 to 11. Kinetic analysis was done as in Section 2.2., with the PSO model resulting in the best fits. As can be seen in Fig. 6, the lower the pH, the more selenite and arsenate are adsorbed. Oxyanions, including arsenate and selenite, tend to become less strongly adsorbed at increasing pH values. This is due to anion adsorption occurring via ligand exchange at hydrous oxide surfaces, in which the adsorbing anions replace the hydroxyl surface groups. The following pH dependent surface complexation reactions occur for up to y = 3 (trivalent) anions (Dzombak and Morel, 1990):

$$XOH + A^{y-} + 3H^+ \overset{K_1}{\leftrightarrow} XH_2A^{3-y} + H_2O \quad (9)$$

$$XOH + A^{y-} + 2H^+ \overset{K_2}{\leftrightarrow} XHA^{2-y} + H_2O \quad (10)$$

Table 4 – Summary of As(V) and Se(IV) removal capacities of goethite in this study and earlier works.

Material	Brunauer–Emmett–Teller surface area (m^2/g)	Initial adsorbate concentrations (mg/L)	pH	Maximum adsorption capacity (mg/g)	Calculation method	Reference
Natural goethite (55%)	13.13	As(V) 0.150	4.0	6.204	Langmuir	This work
		Se(IV) 0.150	4.0	7.740		
Natural goethite (87%)	12.70	As(V) 10–1000	5.5	12.400	Langmuir	Ladeira and Ciminelli, 2004
Natural goethite	2.01	As(V) 0.075–225	7.5	0.452	Langmuir	Giménez et al., 2007
		Se(IV) 0.237–40	4.0	0.521		Rovira et al., 2008
Synthetic goethite	132	As(V) 10–100	3–3.3	45.500	Langmuir	Matis et al., 1997
Synthetic goethite	49.20	Se(IV) 2.450	6.45	8.687	Experiment	Balistrieri and Chao, 1987
Synthetic goethite	70.80	Se(IV) 20	3–7.5	19.980	Experiment	Parida et al., 1997

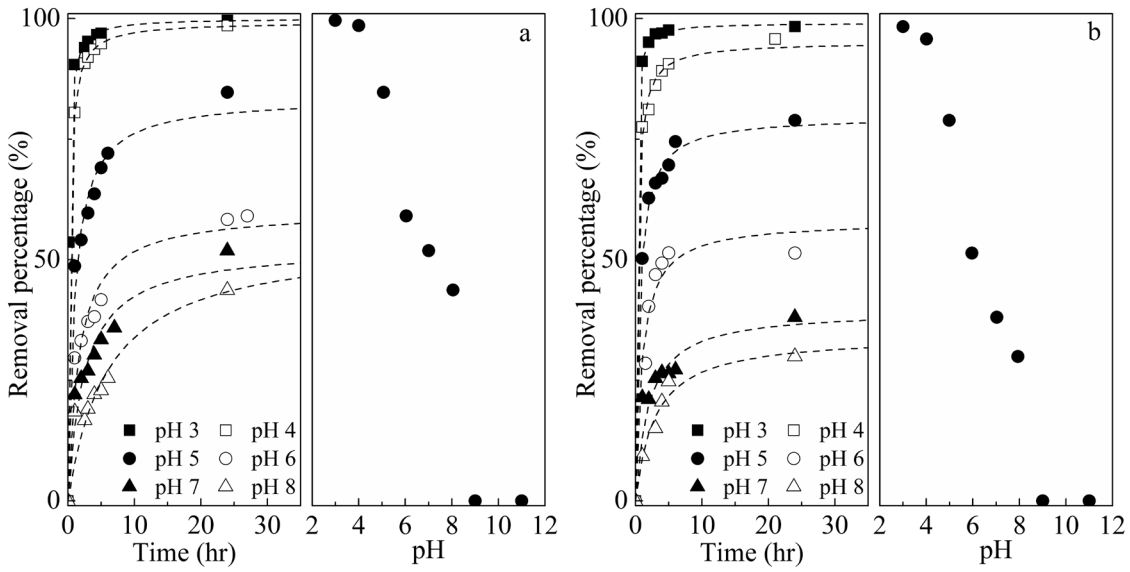

Fig. 6 – pH dependence of (a) arsenate and (b) selenite adsorption at C_0 150 μg/L and 0.333 g/L goethite suspension with PSO kinetic fits.

$$XOH + A^{y-} + H^{+} \overset{K_3}{\leftrightarrow} XA^{1-y} + H_2O \quad (11)$$

$$XOH + A^{y-} \overset{K_4}{\leftrightarrow} XOHA^{y-} \quad (12)$$

where X is a metal (Fe for goethite) and A is an anion. Arsenate (AsO_4^{3-}, y = 3) adsorption occurs through all four reactions above, and selenite (SeO_3^{2-}, y = 2) adsorption occurs via Eqs. (9)–(12). For the reactions above the equilibrium constants (*K*) follow $K_1 > K_2 > K_3 > K_4$; this along with the anion species present results in higher adsorption at lower pH values. Arsenate anions take the form of H_3AsO_4, $H_2AsO_4^-$, $HAsO_4^{2-}$, and AsO_4^{3-} with increasing pH. Similarly, selenite species occur as H_2SeO_3, $HSeO_3^-$, and SeO_3^{2-} with increasing pH. This pH dependency also affects the kinetics of adsorption as can be seen in Table 5 where the kinetic constants decrease with an increasing pH.

2.5. *Leaching/desorption*

Desorption experiments were completed to evaluate the natural goethite samples ability to retain arsenate and selenite in the presence of common anions at varying pH. Phosphate (pH 3 and 7) and hydroxyl (pH 9 and 11) ions were used in this study. Kinetic analysis of desorption was completed using PFO and PSO rate laws applied through non-linear regressions. PFO desorption kinetics (Pan and Xing, 2010) were described via:

$$q_t = (q_a - q_d)e^{-k_1 t} + q_d \quad (13)$$

Table 5 – Kinetic parameters of arsenate and selenite adsorption at varying pH values, C_0 150 μg/L and 0.333 g/L goethite suspension regressed from PSO rate law.

pH	k (g/(mg·hr))	q_e (mg/g)	R_2^2
Arsenate			
2.99	15.9747	0.448	0.9990
4.00	9.576	0.444	1.0000
5.06	3.022	0.339	0.9802
6.04	2.325	0.261	0.9615
7.01	1.754	0.233	0.9401
8.05	0.716	0.231	0.9932
Selenite			
3.00	31.507	0.373	0.9999
4.00	9.899	0.385	0.9973
4.99	4.841	0.346	0.9965
5.96	3.979	0.258	0.9595
7.02	2.644	0.191	0.9797
7.94	2.157	0.160	0.9750

Error for all pH values is ±0.01. q_e: solute adsorbed at equilibrium.

Table 6 – Kinetics parameters for arsenate and selenite desorption regressed using one-parameter non-linear PSO rate law.

pH	k (g/(mg·hr))	q_e (mg/g)	Desorption percentage (%)	R^2
Arsenate				
3.33	5.819	0.289	79.1	0.9187
7.05	2.248	0.161	43.9	0.9349
9.00	14.630	0.084	23.2	0.9565
11.05	18.990	0.154	42.8	0.9084
Selenite				
3.33	8.127	0.335	95.7	0.9262
7.05	1.608	0.303	85.9	0.9586
9.06	4.048	0.169	48.2	0.9684
10.99	39.028	0.312	89.2	0.9753

Solutions at pH 3 and 7 are with 0.1 mol/L PO_4^{3-}.
Error for all pH values is ±0.01.

where q_d (mg/g) is the amount of adsorbate still adsorbed at equilibrium. The PSO desorption model used (Pan and Xing, 2010) was:

$$q_t = \frac{(q_a - q_d)}{1 + k_2 t} + q_d \quad (14)$$

Similar to adsorption, linear, 1-parameter non-linear, and 2-parameter non-linear regressions were applied for both the PFO and PSO models. The 2-parameter non-linear gave the best results, but again the 1-parameter non-linear regressions were chosen due to q_d being known. The PSO model resulted in the highest R^2 values for both arsenate and selenite desorption; therefore it was used to calculate the kinetic values given in Table 6. For phosphate induced desorption of both arsenate and selenite, more desorption occurred at the lower pH. This is due to the same reasons as discussed in Section 2.4 for arsenate and selenite adsorption, as phosphate adsorption follows Eqs. (9)–(12) (PO_4^{3-}, $y = 3$) (Dzombak and Morel, 1990). For desorption by the addition of OH^-, the higher the pH, the higher the arsenate and selenite desorption. This is due to the increase in concentration of OH^- ions in solution. The highest percent desorbed in all the experiments for both selenite and arsenate was under the conditions of 0.1 mol/L phosphate at a pH of 3.33. However, the kinetics of hydroxyl induced desorption are faster than that of phosphate caused desorption. More selenite desorbed than arsenate in all of the experiments. This may be due to arsenate forming inner-sphere complexes while selenite forms a mixture of inner-sphere and outer-sphere complexes on goethite as discussed in Section 2.3.

3. Conclusions

The natural goethite used in this work shows promise as an inexpensive and efficient adsorbent for both arsenate and selenite adsorption. When compared with other As(V) + Se(IV)/goethite systems this works results show lower capacities than that of synthetic goethite samples, however the natural goethite used in this work is cheaper and more readily available. When compared with other natural goethite samples the results vary due to varying natural goethite properties (concentration, surface area, *etc.*) and experimental conditions. The D–R isotherm resulted in the best fit, with the non-linear regressions being superior. Application of the PSO rate law using a non-linear regression resulted in the best fit for both arsenate and selenite adsorption experiments. Adsorption for both selenite and arsenate occurred most efficiently at lower pH values, as expected from previous works. Desorption of arsenate and selenite occurred in the presence of both phosphate and hydroxyl ions and the PSO model gave the best fit for all desorption experiments. The low pH phosphate desorption experiments resulted in the highest amount of arsenate and selenite desorbed, with more selenite desorbed than arsenate. However, the kinetics of hydroxyl induced desorption (pH = 11) were much faster than all other desorption experiments.

Acknowledgments

Authors would like to thank the United States Geological Survey (USGS) (No. 1003073E) as well as the State of Wyoming (No. 1002727A) for providing funding for the research presented.

REFERENCES

Alvarez, M., Sileo, E.E., Rueda, E.H., 2008. Structure and reactivity of synthetic co-substituted goethites. Am. Mineral. 93, 584–590.
Balistrieri, L.S., Chao, T.T., 1987. Selenium adsorption by goethite. Soil Sci. Soc. Am. J. 51, 1145–1151.
Choong, T.S.Y., Chuah, T.G., Robiah, Y., Gregory Koay, F.L., Azni, I., 2007. Arsenic toxicity, health hazards, and removal techniques from water: an overview. Desalin. Water Treat. 217, 139–166.
Dubinin, M., Radushkevich, L., 1947. Equation of the characteristic curve of activated charcoal. Proc. Acad. Sci. Phys. Chem. Sec., USSR55 331-333, 875–890.
Duc, M., Lefevre, G., Fedoroff, M., Jeanjean, J., Rouchaud, J.C., Monteil-Rivera, F., et al., 2003. Sorption of selenium anionic species on apatites and iron oxides from aqueous solutions. J. Environ. Radioact. 70, 61–72.
Dzombak, D.A., Morel, F.Ã.M.M., 1990. Surface Complexation Modeling: Hydrous Ferric Oxide. Wiley.
Environmental Protection Agency, 2016. Aquatic life ambient water quality criterion for selenium — freshwater 2016 — fact sheet. Available:. https://www.epa.gov/wqc/aquatic-life-criterion-selenium, Accessed date: 9 February 2017.
Environmental Protection Agency, 2017a. Chemical contaminant rules. Available:. https://www.epa.gov/dwreginfo/chemical-contaminant-rules, Accessed date: 9 February 2017.
Environmental Protection Agency, 2017b. National primary drinking water regulations. Available:. https://www.epa.gov/ground-water-and-drinking-water/national-primary-drinking-water-regulations, Accessed date: 9 February 2017.
Farmer, V.C., 1974. The Infrared Spectra of Minerals. Mineralogical Society, London.
Foo, K.Y., Hameed, B.H., 2010. Insights into the modeling of adsorption isotherm systems. Chem. Eng. J. 156, 2–10.
Frankenberger Jr., W.T., Benson, S. (Eds.), 1994. Selenium in the Environment. Marcel Dekker Inc., New York.
Freundlich, H.M.F., 1906. Over the adsorption in solution. J. Phys. Chem. 57, 358–471.
Giles, D.E., Mohapatra, M., Issa, T.B., Anand, S., Singh, P., 2011. Iron and aluminium based adsorption strategies for removing arsenic from water. J. Environ. Manag. 92, 3011–3022.
Giménez, J., Martínez, M., de Pablo, J., Rovira, M., Duro, L., 2007. Arsenic sorption onto natural hematite, magnetite, and goethite. J. Hazard. Mater. 141, 575–580.
Golder Associates Inc, 2009. Literature Review of Treatment Technologies to Remove Selenium from Mining Influenced Water (Lakewood, CO, USA).
Ho, Y.S., McKay, G., 1999. Pseudo-second order model for sorption processes. Process Biochem. 34, 451–465.
Ho, Y.S., Porter, J.F., McKay, G., 2002. Equilibrium isotherm studies for the sorption of divalent metal ions onto peat: copper, nickel and lead single component systems. Water Air Soil Pollut. 141, 1–33.
Joint Committee on Powder Diffraction Standards (JCPDS), 1980. Mineral Powder Diffraction File. JCPDS International Centre for Diffraction Data, Swarthmore, PA, USA.
Ladeira, A.C., Ciminelli, V.S., 2004. Adsorption and desorption of arsenic on an oxisol and its constituents. Water Res. 38 (8), 2087–2094.
Lagergren, S., 1898. Zur theorie der sogenannten adsorption gelöster stoffe. Kungliga Svenska Vetenskapsakademiens. Handlingar 24 (4), 1–39.
Langmuir, I., 1916. The constitution and fundamental properties of solids and liquids. Part I. Solids. J. Am. Chem. Soc. 38, 2221–2295.

Matis, K.A., Zouboulis, A.I., Malamas, F.B., Ramos Afonso, M.D., Hudson, M.J., 1997. Flotation removal of As(V) onto goethite. Environ. Pollut. 97, 239–245.

Mohan, D., Pittman Jr., C.U., 2007. Arsenic removal from water/wastewater using adsorbents—a critical review. J. Hazard. Mater. 142, 1–53.

Müller, C.M., Pejcic, B., Esteban, L., Piane, C.D., Raven, M., Mizaikoff, B., 2014. Infrared attenuated total reflectance spectroscopy: an innovative strategy for analyzing mineral components in energy relevant systems. Sci. Rep. 4, 6764.

Pan, B., Xing, B., 2010. Adsorption kinetics of 17α-ethinyl estradiol and bisphenol A on carbon nanomaterials. I. Several concerns regarding pseudo-first order and pseudo-second order models. J. Soils Sediments 10, 838–844.

Parida, K., Gorai, B., Das, N., Rao, S., 1997. Studies on ferric oxide hydroxides: III. Adsorption of selenite (SeO^{2-}_3) on different forms of iron oxyhydroxides. J. Colloid Interface Sci. 185, 355–362.

Prasad, P.S.R., Shiva Prasad, K., Krishna Chaitanya, V., Babu, E.V.S. S.K., Sreedhar, B., Ramana Murthy, S., 2006. In situ FTIR study on the dehydration of natural goethite. J. Asian Earth Sci. 27, 503–511.

Rovira, M., Giménez, J., Martínez, M., Martínez-Lladó, X., de Pablo, J., Martí, V., et al., 2008. Sorption of selenium(IV) and selenium (VI) onto natural iron oxides: goethite and hematite. J. Hazard. Mater. 150, 279–284.

Scott, A., Wild, C., 1991. Transformations and R^2. Am. Stat. 45 (2), 127–129.

Simonin, J.-P., 2016. On the comparison of pseudo-first order and pseudo-second order rate laws in the modeling of adsorption kinetics. Chem. Eng. J. 300, 254–263.

World Health Organization, 2011. Arsenic in drinking-water. Available:. http://www.who.int/water_sanitation_health/dwq/chemicals/arsenic.pdf, Accessed date: 9 February 2017.